Effect of 3D depth on the resolution and the observed image for auto-stereoscopic multi-view 3D display

Hyungki Hong (SID Member)

Abstract — In auto-stereoscopic multi-views, blurring occurs due to the incomplete separation of views for non-zero depths. How this blur affects a 3D image was investigated using the commercial multi-view 3D. The 3D input signal consisted of the square pattern and the gratings of various width and gray level values of G1 and G2. The various combinations of G1 and G2 were used to investigate the dependence of blur on gray G1 and G2 values. The 3D depth caused blurring, which caused a decrease in contrast modulation. Hence, the 3D resolution determined from contrast modulation was affected by the depth and became worse with increasing depth. Therefore, 3D resolution may be used to define the depth range within which the image degradation due to blurring is acceptable. Blur edge width values at the boundaries of gray G1 and G2 were measured and found to be similar irrespective of G1 and G2 values at the same depth. This was because blur was caused by the incomplete separation of views that are independent of G1 and G2. Hence, the blurriness of the observed 3D image is determined only by the depth. The 3D resolution and blur edge width might be useful to characterize the performance of auto-stereoscopic multi-view 3D.

Keywords — *auto-stereoscopic 3D, resolution.*

DOI # 10.1002/jsid.672

1 Introduction

Auto-stereoscopic multi-view 3D is a 3D technology with which the user can perceive the stereoscopic image without special eyeglasses as reported in multiple studies.[1–8] Some studies reported various evaluation and measurement methods for 3D.[9–14]

With the availability of ultra high-definition (UHD) and increasingly advanced display panels that are characterized by high resolutions with a large number of pixels, the number of views for a multi-view 3D image can be increased to obtain a better 3D performance. In multi-view 3D, slanted cylindrical lens sheets are generally used to control the light direction from each subpixel. Because each slanted cylindrical lenslet is on multiple sub-pixels, incomplete image separation of views occurs even at the optimum viewing distance. In auto-stereoscopic multi-view 3D, it was observed that blur at the black–white (B/W) boundary increased as the 3D depth was increased.[15] It was also found that blur edge width (BEW) was related to horizontal disparity between views and the incomplete image separation of views. For 3D resolution, the analysis of resolution in one-dimensional integral imaging using a lenticular sheet had been reported.[16–18] Although a lenticular sheet was used, the principle of auto-stereoscopic multi-view 3D was different from the integral imaging 3D, and the resolution for multi-view 3D needs further research.

A typical 3D image consisted of the various gray levels and the shapes. In this study, the blur effect at the boundaries between the various gray levels and the grating patterns of the various line widths was investigated to understand how it occurred in case of a typical 3D input signal. Because grating patterns were used to define 2D resolution, the effect of blur and depth on 3D resolution was also investigated.[13]

2 Method

When a B/W boundary was used as the 3D input signal in auto-stereoscopic 3D, BEW was found to increase with increasing depth.[15] This phenomenon is related to the incomplete separation of the viewing zones at the user's viewing position. The occurrence of blur at the B/W boundary decreased the image quality of the observed 3D image. The B/W boundary represented an example of a sharp boundary of 3D input signals, which included zero gray levels. The actual image consisted of the various gray levels and the various spatial shapes. The spatial shape could be decomposed into the grating of the various spatial frequencies. Hence, blur at various gray levels and spatial intervals was investigated to understand the blur effect on the general 3D image. A commercial auto-stereoscopic 28-view 3D was used as the sample 3D.[19] In a 28-view 3D

Received 11/03/17; accepted 04/21/18.

The author is with the Department of Optometry, Seoul National University of Science and Technology, Gongneung gil, Nowon-gu, Seoul, Korea; e-mail hyungki.hong@snut.ac.kr.

sample, the slanted lenticular sheet was placed in front of the UHD LCD with a diagonal size of 65 inches and a pixel size of 0.375 mm to make 28 views. The 3D sample was connected to the PC as a UHD monitor. A PC software called "Dimenco 3D player" was used to send the 3D input signal to 3D sample.[19,20] The recommended viewing distance was set to 3 m, and the same viewing zone was repeated horizontally with a period of approximately 32 cm at a viewing distance of 3 m. A pseudoscopic image was also observed at the 3D display with the same horizontal period. The 3D sample supported 3D input signal of stereo 3D, 3D Blu-ray, and 2D + depth map format. Among these, the 2D + depth map format was used as 3D input signal for the experiment.[20] In 2D + depth map format, gray levels of the depth map represented the depth. A gray value of 127 in the depth map represented the depth conditions zero depth that 3D object was located on the screen. Gray values larger and smaller than 127 represented the nearer and farther distance from the screen.

Figure 1 illustrates a 3D input signal that consists of 2D image + depth map format. The 3D input signal consists of a 2D image of 3840 × 2160 pixels and a depth map of 3840 × 2160 pixels. The line thickness of the grating ranged from three and seven pixels. Gray levels G1 and G2 in Fig. 1(a) were selected as 0, 63, 127, 191, and 255. For these five values, 10 combinations of G1 and G2 were possible if G1 and G2 were different. Hence, these combinations were used for a 2D image. The distance between the left boundaries of two adjacent gratings of the 2D image was 192 pixels. In the depth map of Fig. 1(b), nine gray levels were used. Four gray levels with values smaller than 127 were used for four depth conditions D_{fi} behind the screen, and four gray levels with values larger than 127 were used for four depth conditions D_{ni} in front of the screen. The vertical size of each horizontal gray bar shown in Fig. 1(b) was 108 pixels.

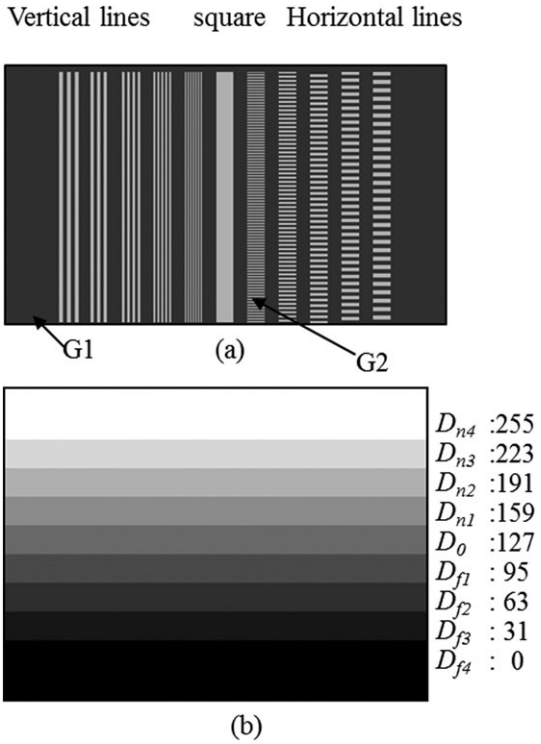

FIGURE 1 — 3D input signal of 2D + depth map format (a) 2D image consisting of a square in the central region and the gratings of various line widths in the uniform background. G1 represents the gray level of background and the dark lines of the grating. G2 represents the gray level of the bright lines of the grating and the square pattern in the center. Gray levels of G1 and G2 are 0, 63, 127, 191, and 255. (b) Depth map consisting of nine gray levels.

The 3D input signal depicted in Fig. 1 was displayed on a 3D sample. For 10 combinations of G1 and G2 of the 3D input signal, all the displayed images were photographed by a camera. The camera was placed on the translation stage where the position and the angle of the camera can be adjusted as shown in Fig. 2. The camera was positioned normal to the 3D sample. If the viewing position was located near the viewing zones of views 1 and 28, the pseudoscopic image would be observed partially or all over the area of 3D screen. The horizontal camera position was selected as the middle of the two viewing positions from which the pseudoscopic image was observed all over the area of 3D screen. At the selected camera position, the pseudoscopic image did not occur at any position of the 3D screen.

The viewing distance was selected as 3 m based on the specification of the commercial 3D sample. The camera of smart phone (G3 of LG Electronics, South Korea) was used. It was set to the standard mode with an enlargement ratio of 8.0. The resolution of the captured image was 4160 × 3120 pixels. In this setup, the camera could not photograph the whole active area of the 3D sample and pixel size of UHD on 3D sample approximately corresponded to 3.5 pixel of the captured image. At a viewing distance of 3 m, the photographed image approximately corresponded to the angular range of 8.4° by 6.35° angles. In the captured image, the positions of the different depth were vertically 0.6° apart, and the adjacent gratings were horizontally 1.05° apart.

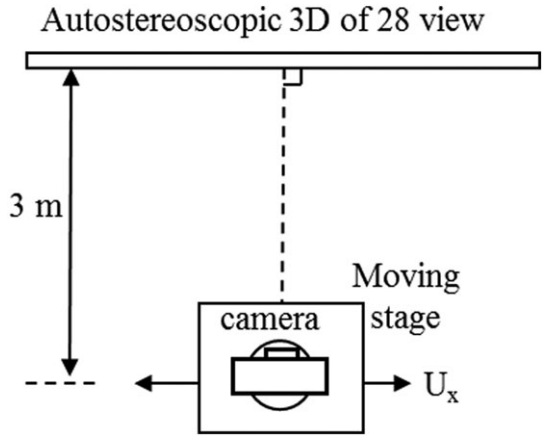

FIGURE 2 — Setup for image capture for auto-stereoscopic 28-view 3D. U_x represents the camera position at a viewing distance of 3 m.

3 Result and analysis

3.1 Resolution

Figure 3(a) shows the images of the square and the grating of horizontal lines of the 3D input signal of Fig. 1, captured in sample 3D at an input signal of G1 = 0 and G2 = 255. A blur effect appeared at G1/G2 boundary of the square pattern along the horizontal direction. The blur width increases with the depth at a large distance. In the images of the gratings of horizontal lines, the blur effect along the vertical direction was not noticeable irrespective of the depth, as illustrated in the relative luminance of Fig. 3(b). The negligible blur along the vertical direction compared with the blur along the horizontal direction is due to the absence of vertical disparity among the adjacent views.[15]

Figure 4(a) shows images of the gratings of the vertical lines of thickness of three, five, and seven pixels of 3D input signal at G1 = 0 and G2 = 255. Compared with the horizontal lines shown in Fig. 3, the occurrence of blur was noticeable. Contrast between the bright and dark lines decreased with increasing depth due to the blur effect. Distinguishing the grating was difficult for lines of smaller thickness compared

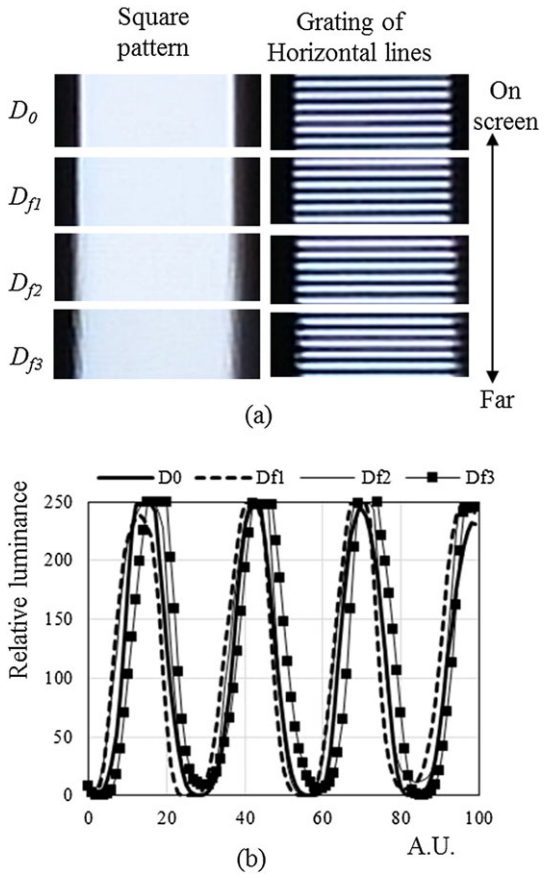

FIGURE 3 — (a) Captured images of square pattern and gratings of horizontal lines of 3D input signal shown in Fig. 1 with line thickness of seven pixels at G1 = 0 and G2 = 255. Depth increased toward the lower images. (b) Relative luminance distribution along the vertical cross section of the image of line thickness of seven pixels. Horizontal and vertical axes represent the vertical positions in the image and the relative luminance.

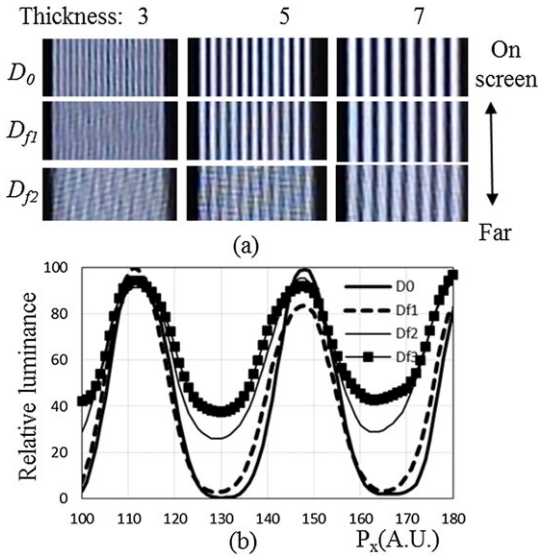

FIGURE 4 — Grating of the vertical lines at G1 = 0 and G2 = 255. (a) Captured image of grating at line thickness of three, five, and seven pixels. (b) Luminance distribution along the horizontal cross section of the image at a line thickness of five pixels. P_x represents the horizontal coordinates of the image in arbitrary units.

with the lines of larger thickness. Figure 4(b) illustrates the relative luminance distribution along the horizontal cross section of the image for a line thickness of five pixels at the grating of G1 = 0 and G2 = 255. Relative luminance was derived from the gray G_p of each pixel of the image. A gamma value of 2.2 was assumed, and the relative luminance was calculated using Eq. (1).

$$Lum(G_p) = \left({}^{G_p}/_{255}\right)^{2.2} \tag{1}$$

Gray G_p values of 255, 191, 127, and 63 corresponded to the relative luminance of 100%, 53%, 21.6%, and 4.6%, respectively, at the gamma value of 2.2.

Various methods of defining the resolution using contrast modulation (CM) or modulation transfer function have been reported.[13] In using CM, 2D resolution was defined as the smallest line thickness of the grating in which CM was larger than 50%. The CM is defined by Eq. (2) where $L_{\max}$ and $L_{\min}$ represent the luminance of the bright and dark lines of the grating.

$$CM = \frac{L_{\max} - L_{\min}}{L_{\max} + L_{\min}}. \tag{2}$$

As observed in Fig. 4(b), $L_{\min}$ tended to increase at larger depths, which means a corresponding decrease of CM. The resolution of 3D display seen by each eye can be considered to be identical to the 2D resolution although the binocular 3D resolution might be different from 2D resolution.

To investigate the effect of depth on 3D resolution, CM was calculated for grating of G1 = 0 and G2 = 255. Figure 5 illustrates CM and images of gratings of vertical lines for

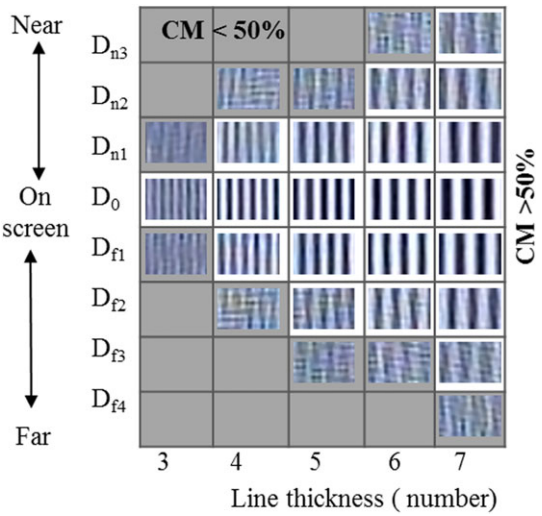

FIGURE 5 — CM and captured images of grating at 3D image of G1 = 0 and G2 = 255. Horizontal and vertical directions represent the line thickness of grating and depth conditions. The gray area represents the conditions that CM is smaller than 50%. CM, contrast modulation.

various conditions of depth and line thickness. As CM decreased at larger depths, a larger line thickness was needed for CM to be larger than 50%. Figure 5 illustrates that the 3D resolution for each eye along the horizontal direction depended on the depth. For the calculation of CM in Fig. 5, data from the images captured by the camera were used. Hence, quantitative reliability of data was limited compared with that of the data measured by a 2D luminance meter. Hence, the exact value of CM may be different if a 2D luminance meter was used. However, the trends of change in the 3D resolution corresponding to depth would remain the same. As 3D resolution became larger at larger depths, the image quality of the observed 3D image would also become worse. If a specific size of a 3D resolution is selected as the acceptable limit, this may in turn be used to define the acceptable range of the depth.

3.2 Blur at boundary of two gray levels

Figure 6 shows images of the left boundary of a square pattern located at the center of a 3D input signal at the various values of G1 and G2. In each image, dark and bright areas corresponded to G1 and G2, respectively. Blur in Fig. 6 increased at larger depth irrespective of G1 and G2. Figure 7(a) illustrates the relative luminance distribution along the horizontal cross section around the left boundary of the square pattern for various values of G1 and G2 at a depth of D_{f2}. For G1 and G2, luminance at the left and right edges of Fig. 7(a) were defined as L_{G1} and L_{G2}, and 10% and 90% luminance with respect to these luminance values of L_{G1} and L_{G2} for G1 and G2 were defined as

$$L_{10\%}(G1, G2) = 0.1(L_{G2} - L_{G1}) + L_{G1}, \quad (3a)$$

$$L_{90\%}(G1, G2) = 0.9(L_{G2} - L_{G1}) + L_{G1}. \quad (3b)$$

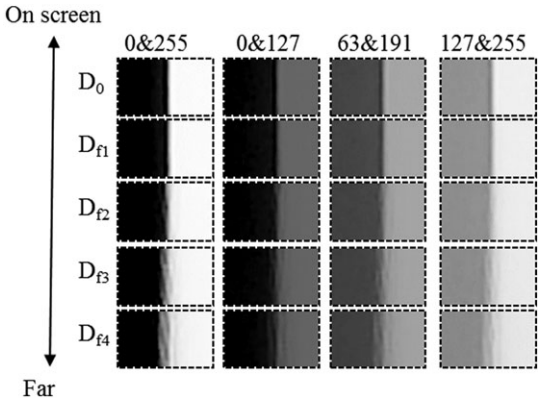

FIGURE 6 — Captured images of the left boundary of the square pattern at the various G1 and G2 values. Two numbers on the top of each image represent G1 and G2.

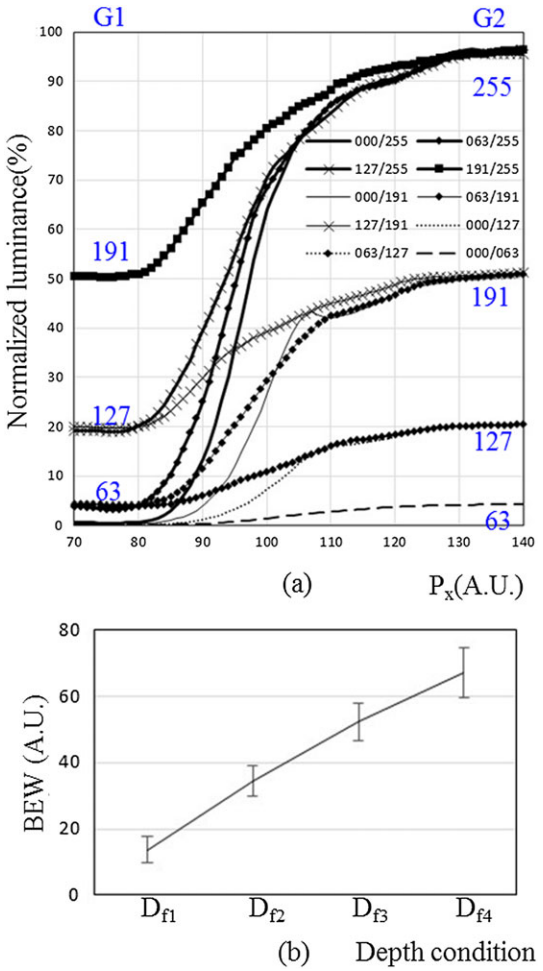

FIGURE 7 — (a) Luminance distribution along the horizontal cross section of the image around the left boundary of the square pattern at a depth condition of D_{f2}. Numbers on the left and right represent gray levels of G1 and G2. P_x represents the horizontal coordinate of the image in arbitrary units. (b) Average of BEW for the 10 combinations of G1 and G2. Horizontal and vertical axes represent the depth and BEW. BEW, blur edge width.

Blur edge width was defined as the distance between two positions of 10% luminance and 90% luminance for the grays of G1 and G2.[13,15] BEW values around the left

boundary of the square pattern were calculated for all the values of G1, G2, and depth. Figure 7(b) illustrates the average of BEW for 10 combinations of G1 and G2 at each depth conditions. Small standard deviation at each condition of Fig. 7(b) implies the similar BEW irrespective of conditions of G1 and G2.

Figure 8 illustrates the schematic concept to explain the blur effect in multi-view 3D due to incomplete image separation. Figure 8(a) illustrates the images for each view for the 3D image at non-zero depth. At non-zero depth, the white squares for each view are at horizontally different positions, inducing a perception of depth. Figure 8(b) illustrates the image seen at the viewing zone of view n. Luminance by image of view n is the strongest. Due to incomplete image separation of viewing zones of multi-view 3D, the image from the adjacent view n ± m also contributes to the luminance. In Fig. 8, m is assumed to be 2 although m can be any other integer. As white squares of view n, n ± 1, n ± 2 are at different positions, blur appears at B/W and W/B boundaries. The function $f_b(x)$ in Fig. 8(c) represents the blur effect at boundaries between the area of zero gray and the area of normalized luminance of 100%. This function is determined by the characteristics of the incomplete separation of views of auto-stereoscopic 3D. By multiplying the luminance of any gray level to this function, the blur effect between the areas of zero gray and any gray other than zero gray can be represented. Similarly, the function $f'_b(x)$ in Fig. 8(c) represents the blur effect at boundaries between the areas of normalized luminance of 100% and the area of zero gray. The blur width is related to the depth and incomplete image separation.[15] If the characteristics of incomplete image separation of 3D display for view n are symmetric with respect to ± m, $f'_b(x)$ is equal to 1- $f_b(x)$.

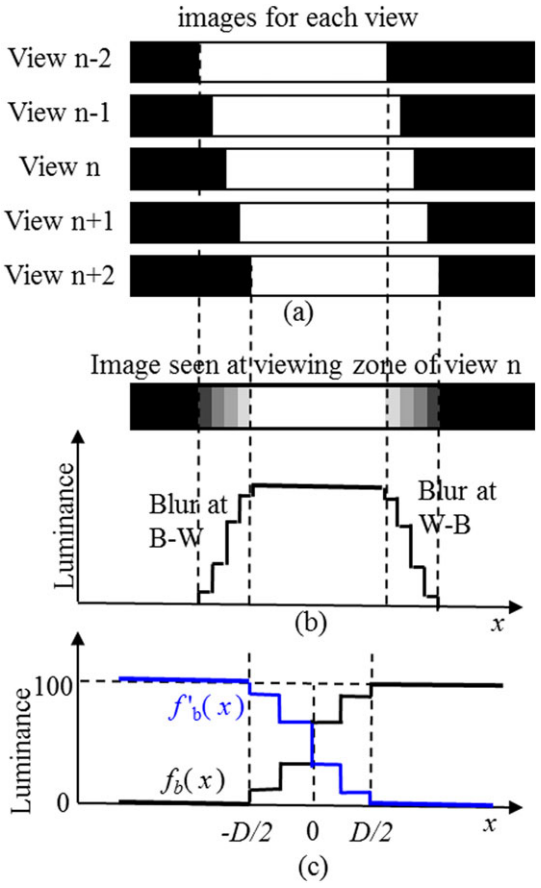

FIGURE 8 — Schematic concept to explain blur effect in multi-view 3D due to incomplete image separation. 3D image is white square pattern of the non-zero depth over a black background. (a) Images for each view. (b) 3D image seen in the viewing zone of view n. x represents the horizontal coordinates on 3D display. (c) Blur effects at B/W (black/white) and W/B boundaries are represented as function $f_b(x)$ and $f'_b(x)$. *D* relates to the horizontal disparity to induce depth and the characteristics of incomplete image separation of multi-view 3D display.

Figure 9 illustrates the schematic concept to explain the BEW at G1 and G2 boundaries of the 3D input signal. The boundary between G1 and G2 at non-zero depth can be decomposed into the boundary between G1 and black and the boundary between black and G2 as illustrated in Fig. 9(b,c). The blur effect at G1 and G2 boundaries can then be expressed as the sum of blur at these two boundaries.

$$L_{G1} \times f'_b(x) + L_{G2} \times f_b(x).$$

As $f'_b(x)$ is equal to 1- $f_b(x)$, this expression can be written as

$$L_{G1} + (L_{G2} - L_{G1}) \times f_b(x).$$

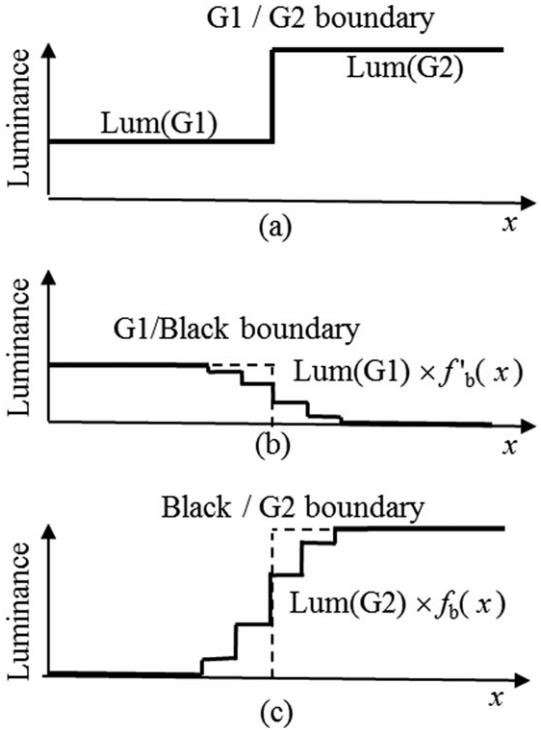

FIGURE 9 — Blur at G1 and G2 boundary of 3D input signal of non-zero depth. (a) 3D input signal of G1 and G2 boundary. (b) Blur at G1 and black boundary. (c) Blur at black and G2 boundary.

The above-mentioned expression shows that blur effect at G1 and G2 boundaries was still determined by the function $f_b(x)$ but was independent of G1 and G2 as the function $f_b(x)$ did not depend on G1 and G2.

This schematic analysis can explain why the blur effect and BEW for the same depth was independent of G1 and G2 values. Hence, the observed image would be affected by blur irrespective of the grays of the 3D input signal.

4 Conclusion

In a sample of an auto-stereoscopic multi-view 3D, a slanted lenticular lens was used and the separation of views was incomplete. For this optical configuration, the blur effect is dependent on the depth along the horizontal direction. For example, from the selected auto-stereoscopic 3D sample, the B/W grating of three-line thickness was distinguishable at the conditions of the zero depth but a B/W grating of seven-line thickness was difficult to distinguish at the farthest distance. The 3D resolution for each eye can be determined from the CM values of black and white gratings, similar to the measurement of 2D resolution. As the blur effect affected CM values, 3D resolution was measured and it was found to depend on the depth along the horizontal direction.

Blur edge width values at the boundaries of gray G1 and G2 were found to steadily increase with increasing depth. However, BEW values at the same depth were almost the same, irrespective of the values of G1 and G2, as illustrated in Fig. 7(b). A schematic analysis of Fig. 9 and expression of blur effect at G1 and G2 boundaries showed the reason for no dependence of BEW on G1 and G2.

3D resolution and BEW at the boundaries of gray G1 and G2 directly affect the image seen by the viewer. Hence, these might be useful for characterizing the performance of auto-stereoscopic multi-view 3D. The 3D resolution may be used to define the depth range that image degradation due to blurring is acceptable.

Acknowledgments

This research was supported by the Research Program funded by the Seoul National University of Science and Technology.

References

1 T. Okoshi, Three Dimensional Images Techniques. Academic Press, New York, (1976).
2 C. van Berkel, "Image preparation for 3D-LCD," *Proc. SPIE*, **3639**, 84–91 (1999).
3 B. Javidi and F. Okano, Three-Dimensional Television, Video and Display Technologies. Springer, New York, (2002).
4 J. Y. Son and B. Javidi, "Three-dimensional imaging method based on multi-view images," *J. Disp. Technol.*, **1**, 125–140 (2005).
5 H. K. Hong *et al.*, "Electric-field-driven LC lens for 3-D/2-D autostereoscopic display," *JSID*, **17**, 399–406 (2009).
6 Y. Takaki, "Multi-view 3-D display employing a flat-panel display with slanted pixel arrangement," *JSID*, **18**, 476–482 (2010).
7 J. Kim *et al.*, "Lenticular lens array based on liquid crystal with a polarization-dependent focusing effect for 2D–3D image applications," *J. Inf. Disp.*, **16**, 11–15 (2015).
8 H. K. Hong, "Analysis of the dependence of the viewing zones on the display radius in autostereoscopic 2 view displays of horizontally concave surface," *J. Disp. Technol.*, **12**, 808–814 (2016).
9 M. Salmimaa and T. Järvenpää, "3-D crosstalk and luminance uniformity from angular luminance profiles of multi-view auto-stereoscopic 3-D displays," *JSID*, **16**, 1033–1040 (2008).
10 A. Yuuki *et al.*, "Influence of 3-D cross-talk on qualified viewing spaces in two- and multi-view autostereoscopic displays," *JSID*, **18**, 483–493 (2010).
11 A. Abileah, "3-D displays – Technologies and testing methods," *JSID*, **19**, 749–763 (2011).
12 S. M. Jung *et al.*, "New characterization of 3D performance for multi-view auto-stereoscopic displays," *SID Symp. Dig.*, **43**, 1155–1158 (2012).
13 ICDM (International Committee for Display Metrology) IDSM (Information Display Measurement Standard), http://www.icdm-sid.org/downloads/idms1.html, Accessed December 2016.
14 International Electro-technical Commission "IEC 62629–22-1: 3D display devices – Part 22–1: measuring methods for auto-stereoscopic displays-optical, Edition 2" (2016).
15 H. K. Hong, "Influence of depth and 3D crosstalk on blur in multi-view 3D displays," *JSID*, **25**, 450–457 (2017).
16 H. Hoshino *et al.*, "Analysis of resolution limitation of integral photography," *J. Opt. Soc. Am. A*, **15**, 2059–2065 (1998).
17 T. Saishu and K. Taira, "Resolution analysis of lenticular-sheet 3D display system," *Proc. SPIE*, **6778**, 67780E1–8 (2007).
18 T. Saishu, "Resolution measurement of autostereoscopic 3-D displays with lenticular sheet," *Proc. IDRC*, 233–236 (2008).
19 Skymedia 28view "skymedia.com", accessed Nov, 2016.
20 Dimenco 2D-plus-Depth "https://www.dimenco.eu/downloads/DIM-2DZ-manual.pdf", Accessed August 2017.

Hyungki Hong is an associate professor at the Department of Visual Optics, Seoul National University of Science and Technology since 2010 and a member of SID. He received his BS in Physics in Seoul National University and PhD in Physics from Korea Institute of Science and Technology (KAIST). After receiving his PhD in 1998, he joined LG Display (at that time LCD division of LG Electronics) and worked for the performance improvement and the performance characterization of LCD and 3D display until 2010. His research interest is human factors related to displays such as 3D and VR.